Particle Tracking in the BSF Beamline

T.ADACHI

National Laboratory for High Energy Physics
1-1 Oho, Tsukuba-shi, Ibaraki-ken, 305, Japan

Abstract

A particle-tracking program for transverse motion was developed. It is used to calculate the particle trajectory affected by dipole and quadrupole magnetic fields. The calculation also considers multiple Coulomb scattering and energy loss in matter. The program was applied to a transport line for a 500-MeV proton beam. The result was compared with beam profiles and residual radioactivities measured along the beamline.

I. Introduction

It has become a serious problem to prevent the activation of accelerator components due to beam loss according to the increment of the beam intensity. A beam comprises core and a halo. The beam core is completely characterized in the frame of the equation of motion; it can also be defined using a few parameters. On the other hand, the beam halo cannot be defined well since it may be generated from the beam core by some stochastic processes; i.e. multiple Coulomb scattering and energy loss in matter. In a synchrotron, the stripping foil for H^- injection is the main generator of the halo. A profile monitor of secondary emission type is a candidate in a beam transport line. Such a beam halo escapes from the confining region easily and causes beam loss. In addition, the beam core may also escape from an aperture by blowing up through electro-magnetic interaction; i.e. direct space charge and instabilities. Therefore, in order to consider the behavior of a beam, both stochastic and electro-magnetic processes must necessarily be considered.

We are now developing a beam simulation program which calculates a particle trajectory affected by the dipole and quadrupole magnetic fields. The calculation also contains multiple Coulomb scattering and energy loss in matter by using a Monte Carlo method. Though we plan to include the effect of a static electric potential in the transverse plane, it has not been completed yet. This program was applied to the beam transport line which supplies a 500MeV proton beam to the beam dump, neutron, meson and medical facilities (BSF beamline). The result was compared with the beam profiles and residual radioactivities along the beamline. The beam profiles were in good agreement with the simulation. The major hot points of the beamline almost coincided with the simulation, and the

radiation level was also proportional to the calculated beam loss rate.

II. Tracking Program

§1 General

The program comprises two parts. One calculates a transfer matrix for each element as well as the twiss parameters, dispersions and momentum compaction factor if a periodic machine is selected (TRACK13). The other simulates beam trajectories taking into account of the materials and apertures (TRACK14). Those boundaries are defined by polygons using up to 20 points.

A particle is transported successively from the first element to the last element. In the periodic case, a particle is reinjected to the first element. The elements are defined by some parameters: i.e. the element name, as well as the kind of element, length, deflection angle, field gradient and aperture information . In matter, the energy loss and multiple Coulomb scattering are considered in terms of Landau and Moliere theories.[1,2] At the exit of each element, the particle position is sensed whether it stays inside or outside the aperture. When the particle is outside the aperture, it is considered to be dead.

§2 Incident Beam

The incident beam is assumed to have an elliptic boundary with a major axis of A and minor axis of B in the transverse plane, where

$$A=n\sqrt{\varepsilon_x\beta_x} \quad \text{and} \quad B=n\sqrt{\varepsilon_y\beta_y}. \tag{1}$$

Assuming that the beam profile has a Gaussian form, both the emittances, ε_x and ε_y, correspond to 2-σ beam widths. We chose 2 as the value of n, so that 99.994% of the Gaussian beam is included.

In order to assure that motions in the horizontal and vertical phase planes are independent of each other, the single-emittance model must be discarded since independent motion with single emittance in each phase plane gives a Lissajous trajectory with a rectangular envelope in the transverse plane (Fig. 1). Therefore, we adopted the following algorithm in order to obtain the particle state (x,x',y,y'). When a point (x,y) is given inside the ellipse, the allowed amplitudes are first calculated by a Monte Carlo method using the following equations:

$$\begin{aligned}
&Z_j=((-b_j-(b_j^2-4a_j(c_j+S\eta_j/2))^{1/2})/2a_j)^{1/2} \quad (j=1,2),\\
&a_1=B^2/4A^2, \qquad a_2=A^2/4B^2,\\
&b_1=-(B^2-y^2)/2, \quad b_2=-(A^2-x^2)/2,\\
&c_1=-B^2x^4/4A^2+(B^2-y^2)x^2/2,\\
&c_2=-A^2y^4/4B^2+(A^2-x^2)y^2/2
\end{aligned} \tag{2}$$

and

$$S=2a_1x^4+2a_2y^4+x^2y^2-A^2y^2-B^2x^2+A^2B^2/2,$$

where Z_1(=X) and Z_2(=Y) denote the allowed betatron amplitudes of the horizontal and vertical motions, whose trajectories pass through the point (x,y); S denotes the total area of the possible rectangles,

including point (x,y), and η_j denotes a uniform random number within a range of o to 1. Here, the two-dimensional probability density of the betatron amplitudes X and Y is assumed to be proportional to the rectangular area 4XY. Once a group of X and Y is selected among possible amplitudes, (x,x') or (y,y') is given as a point inside the ellipse in each phase plane determined with twiss parameters and emittance Z_j^2/β_j by using a uniform random number.

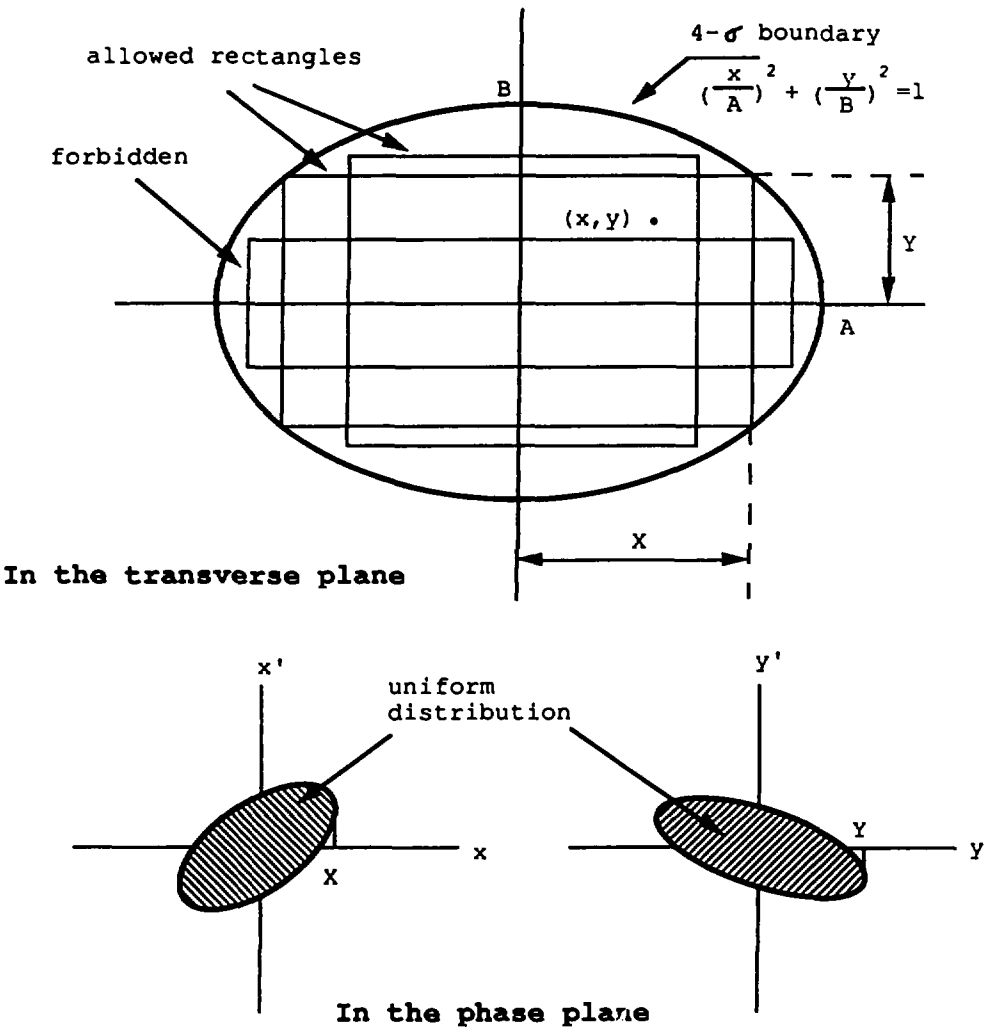

Fig. 1 Beam structure in the transverse plane and phase plane.

The momentum deviation, $\Delta p/p$, is generated so as to have an elliptic distribution given by

$$f(\delta)=2*(1-(\delta/\delta_0)^2)^{1/2}/\pi, \qquad (3)$$

where δ is the momentum deviation ($=\Delta p/p$) and δ_0 is the maximum momentum deviation.

§3 Elements

The program can deal with the following elements: drift space, the sector magnet, its edge, the quadrupole magnet, and a magnet of combined type. These elements are interpreted to transfer matrices.[3] A 'Kick' element affects the beam by changing only its direction. The 'matter' option causes multiple scattering and energy loss of a particle by the Monte Carlo method. An auxiliary 'Monit' option creates histograms of horizontal and vertical beam profiles at the location where this option is found. These elements are described below.

3-1 Drift Space : DRIFT

A transfer matrix for a drift space is defined by

$$M_{ij}=\begin{vmatrix} 1 & s & 0 \\ 0 & 1 & 0 \\ 0 & 0 & 1 \end{vmatrix}, \qquad (4)$$

where s denotes length of the drift space.

3-2 Sector Magnet : HSECT and VSECT

A transfer matrix for a sector magnet is defined by

$$M_{ij}=\begin{vmatrix} \cos\theta & \rho\sin\theta & \rho(1-\cos\theta) \\ -\sin\theta/\rho & \cos\theta & \sin\theta \\ 0 & 0 & 1 \end{vmatrix}, \qquad (5)$$

where θ denotes the deflection angle and ρ the bending radius. In a plane perpendicular to the deflection plane, the transfer matrix is the same as that for drift space by substituting $\rho\theta$ to s.

3-3 Magnet edge : HEDGE and VEDGE

A transfer matrix for a magnet edge is defined by

$$M_{ij}=\begin{vmatrix} 1 & 0 & 0 \\ \tan\varepsilon/\rho & 1 & 0 \\ 0 & 0 & 1 \end{vmatrix}, \qquad (6)$$

where ε denotes an angle between the direction of the bending radius, ρ, and the pole face. In a plane perpendicular to deflection plane, the transfer matrix is defined by

$$M_{ij}=\begin{vmatrix} 1 & 0 & 0 \\ (b/6\rho\cos\varepsilon-\tan\varepsilon)/\rho & 1 & 0 \\ 0 & 0 & 1 \end{vmatrix}, \qquad (7)$$

where b denotes the range of the fringing field by a linear approximation.

3-4 Magnet of combined type : FCMB and DCMB

The transfer matrix of the combined-type magnet is defined by

$$M_{ij}=\begin{vmatrix} \cos\zeta & \sin\zeta/\sqrt{k} & (1-\cos\zeta)/\rho k \\ -\sqrt{k}\sin\zeta & \cos\zeta & \sin\zeta/\rho\sqrt{k} \\ 0 & 0 & 1 \end{vmatrix} \qquad (8)$$

in the focusing plane, where $k=(|n|+1)/\rho^2$ is for the horizontal plane, $k=|n|/\rho^2$ for vertical plane and $\zeta=s\sqrt{k}$. The transfer matrix for vertical plane is

$$M_{ij}=\begin{vmatrix} \cosh\zeta & \sinh\zeta/\sqrt{k} & (\cos\zeta-1)/\rho k \\ \sqrt{k}\sinh\zeta & \cosh\zeta & \sinh\zeta/\rho\sqrt{k} \\ 0 & 0 & 1 \end{vmatrix} , \qquad (9)$$

where $k=(|n|-1)/\rho^2$ is for the horizontal plane, $k=|n|/\rho^2$ for vertical plane and $\zeta=s\sqrt{k}$.

3-5 Quadrupole Magnet : QF and QD

The transfer matrices for quadrupole magnet are obtained from the transfer matrices for the combined-type magnet by setting $k=g/B\rho$ and $1/\rho=0$.

3-6 Kick : KICK

This element cannot be represented by a transfer matrix. When this element is found, the state vector (x,x') changes to (x,x'+θ). Here, θ denotes the kick angle.

3-7 Matter : MATTER

This element causes some deflection and displacement due to multiple Coulomb scattering as well as energy loss. The amount of energy loss is calculated in terms of Landau theory.[1] In thin matter, the energy transfer for each collision is calculated.[4] At the same time, multiple Coulomb scattering is also calculated as a succession of small-angle Rutherford scattering with a screening effect. For a thick matter, Moliere theory is adopted.[2] In order to save the CPU time, Landau distribution and a Moliere's distribution are tabulated precedently by the following formulations:

(i) Landau distribution

$$F(\lambda)=\int_{C-i\infty}^{C+i\infty}\exp(\eta\mathrm{Log}\eta+\eta\lambda)d\eta \qquad (10)$$

$$\lambda=(\Delta-\Delta_{prob})/\xi \quad ,$$

where Δ is the energy loss and $\xi=0.1536(Z/A)\rho t/\beta^2$ (MeV), using atomic number Z, mass number A, density ρ and thickness t of matter for a proton with a velocity β. The most probable energy loss, Δ_{prob}, is given by

$$\Delta_{prob}=\xi(\mathrm{Log}(2\xi m_e c^2\beta^2\gamma^2/I^2)-\beta^2+0.4228-\delta), \qquad (11)$$

where $m_e c^2$ is the electron rest mass, I the mean excitation potential of matter and δ a parameter used for density correction. The value of δ for each atom was quoted from Sternheimer's works.[5]

(ii) Moliere's distribution

$$F(\theta)=\int_0^\infty \exp(\Omega(\chi)-\Omega_0)\,J_0(\chi\theta)\,\chi d\chi \qquad (12)$$

$$\Omega(\chi)-\Omega_0=\chi^2\mathrm{Log}(0.29175\chi^2/\nu)/4,$$

where θ is a normalized polar angle measured with respect to the direction of an incident particle, and ν is the average collision number. The same equation gives a normalized lateral displacement upon replacing ν with 0.6492447ν. Both the actual scattering angle (θ_x, θ_y) and the displacement (x,y) are given by the following relations:

$$\theta_x=\theta\theta_c\cos\phi_1,\ \theta_y=\theta\theta_c\sin\phi_1,\ x=\theta R_c\cos\phi_2 \text{ and } y=\theta R_c\sin\phi_2, \qquad (13)$$

where ϕ_1 and ϕ_2 are azimuthal angles distributed uniformly in a range between 0 and 2π. θ_c and R_c are defined by $\theta_c^2=\pi nt(2Ze^2/p\beta)^2$ and $R_c^2=t^2\theta_c^2/3$, respectively, using the particle density, n; the thickness, t; and the atomic number, Z, of the matter. The proton momentum is p and the velocity β.

3-8 Monitor option : MONIT

This element is treated as a drift space. When it is found, the horizontal and vertical profiles are created within a range between -50mm and 50mm.

III. Simulation

The program was applied to the BSF beamline. This beamline supplies a 500-MeV proton beam from a Booster synchrotron to four experimental halls: neutron, meson, medical and dump facilities. Fig. 2 shows a plan view of the beamline. Beam tracking from the entrance of the BSF beamline to the neutron facility is described below.

There are 32 quadrupole magnets, 5 dipole magnets and 19 steering magnets in this line. The calculation took into account only the quadrupole and dipole magnets. The steering magnets were treated as drift space. The beam profile monitors were considered as being a generator of the beam halo (matter option). The incident beam was generated by using twiss parameters mapped to the entrance of the beamline from the exit of the Booster. The emittances were adjusted so as to reproduce the actual beam profiles at the point of the first beam profile monitor (PR01) where dispersion was not so large. The maximum momentum deviation, δ_0, used in equation (3) was determined to be 0.4% in order to fit all of the profiles of the beamline. The beam profile monitor is a secondary-emission type and comprises 32 tungsten wires of 30μm in diameter with a 2.5mm pitch for horizontal profile measurements. The same number of wires are used for vertical profile measurements. These wires and a ceramic frame are the main scatterers of the beam. In a simulation, the wire was considered to be a square pillar.

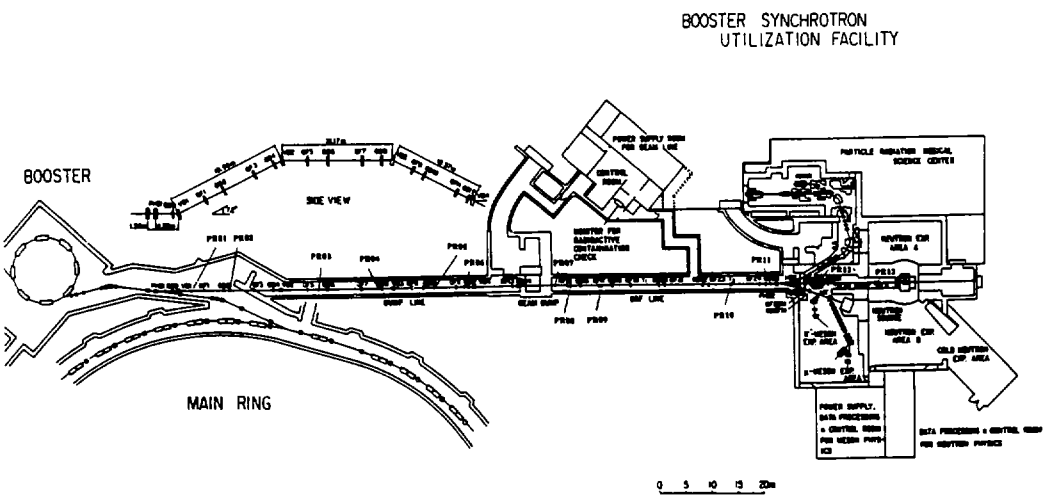

Fig. 2 Plan view of the BSF beamline.

The calculations were performed for two cases: with and without profile monitors. In the former case, the total amount of beam loss was about 1% of incident beam intensity. The latter gave a very small loss, less than 10^{-4}. This result implies that the beam halo is generated by profile monitors and is the main origin of residual radioactivity in the beamline, rather than orbit distortion. In order to test our speculation, we are planning to remove the profile monitors from the beamline during the next machine cycle.

Fig.3 compares the calculated profiles with the actual beam profiles at each monitoring point, where the line and the histogram denote the calculation and measurement, respectively. As shown, the simulation is in good agreement with the measurement, except for horizontal profile of PR13.

The beam loss count along the beamline is shown in Fig.4, together with a measurement of the radio activities (relative values). In this figure, the left edge of the knife shape histogram represents the value of relative exposure or loss count at an entrance of the element. The right edge represents the value at an exit of the element. The open and solid histograms correspond to the relative exposure and the calculated beam loss count, respectively. As shown, the major hot points almost coincide with the simulation, and the exposure level is also proportional to the calculated loss count. At the first five elements (PHB1 to ST2H), the calculation gave no beam loss. These points may occur due to orbit distortion. This will be also clarified by the next beamline study.

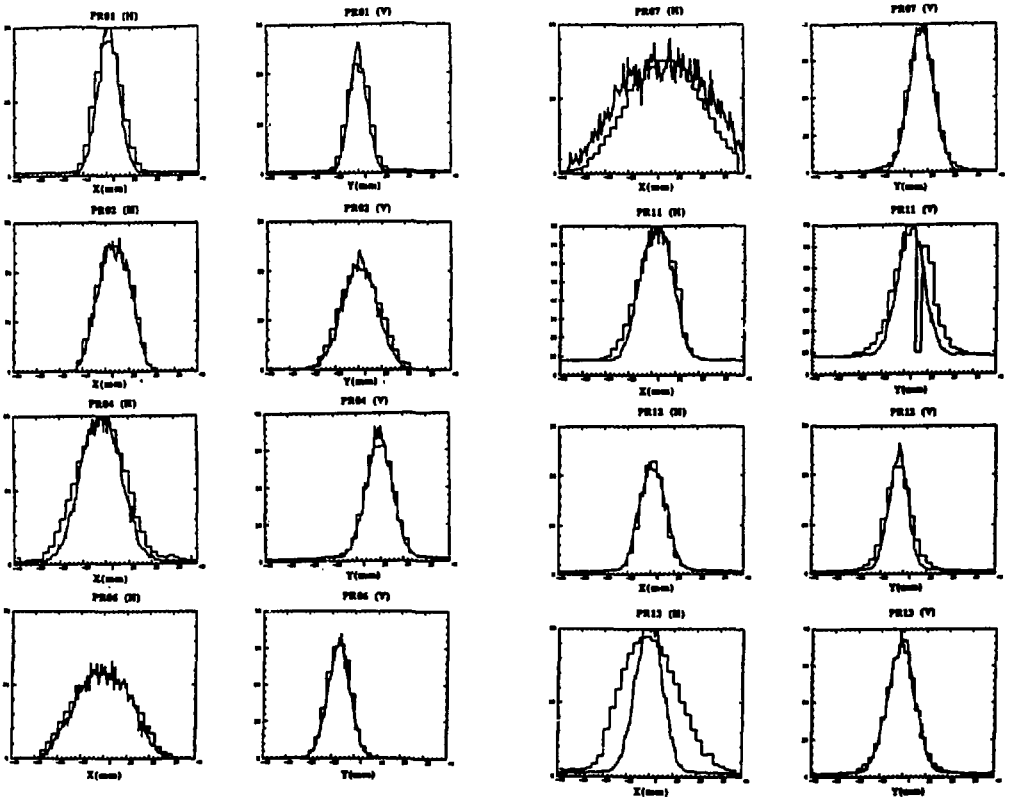

Fig. 3 Comparison between measured profiles and simulation.

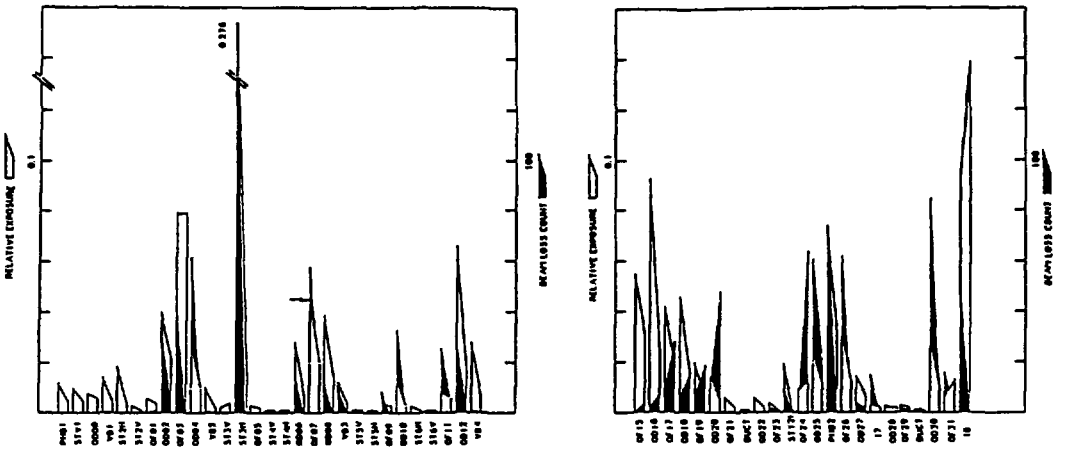

Fig. 4 Beam loss count along the beamline.

IV. Remarks

This program was applied to the BSF beamline and reproduced the actual beam profile successfully, except for the horizontal profile of PR13. The major hot points of the beamline are also consistent with measurements. This calculation implies that the tungsten wires of the beam profile monitors are the main origin of the beam halo. This idea will be tested next machine cycle by removing the profile monitors.

Acknowledgement

The author would like to thank Dr. Irie for useful discussion and continuous encouragement and Mr. Yano for useful information on the beam profiles of the BSF beamline.

References

1. L.Landau, J.Phys.USSR 8,201 (1944).
2. W.T.Scott, Revs.Mod.Phys. 35,231 (1963).
3. C.Bovet et.al, CERN/MPS-SI/Int. DL/70/4 (1970).
4. K.A.Ispirian et.al, Nucl.Instr. and Meth. 117,125 (1974).
5. R.M.Sternheimer, Phys.Rev. 145,247 (1966), 164,349 (1967) and B3,3681 (1971).